Dawoud, D. W., Héliot, F., Imran, M. A. and Tafazolli, R. (2020) A novel unipolar transmission scheme for visible light communication. IEEE Transactions on Communications, 68(4), pp. 2426-2437.

A Novel Unipolar Transmission Scheme for Visible Light Communication

Diana W. Dawoud, Fabien Héliot, Muhammad Ali Imran, and Rahim Tafazolli,

Abstract

This paper proposes a novel unipolar transceiver for visible light communication (VLC) by using orthogonal waveforms (OWs). The main feature and advantage of our proposed scheme over most of the existing unipolar schemes in the literature is that the polarity of the real-valued orthogonal frequency division multiplexing (OFDM) sample determines the pule shape of the continuous-time signal and thus, the unipolar conversion is performed directly in the analog domain and not in the digital domain. Therefore, our proposed scheme does not require any direct current (DC) bias or clipping as it is the case with existing schemes in the literature. The bit error rate (BER) performance of our proposed scheme is analytically derived and its accuracy is verified by using Matlab simulations. Simulation results also substantiate the potential performance gains of our proposed scheme against the state-of-the-art OFDM-based systems in VLC. For instance, it is shown that the absence of DC shift and clipping in our scheme supports more reliable communication and outperforms both the asymmetrically clipped optical-OFDM (ACO-OFDM) and direct-current optical-OFDM (DCO-OFDM) by at least 3 dB and 2 dB, respectively, in terms of the required signal to noise ratio to achieve a target bit error rate (BER) of 10^{-4} when considering the same spectral efficiency for all the schemes.

D. W. Dawoud, F. Héliot and R. Tafazolli are with University of Surrey, UK (e-mail: d.dawoud@surrey.ac.uk; f.heliot@surrey.ac.uk; r.tafazolli@surrey.ac.uk).

Muhammad Ali Imran is with School of Engineering, University of Glasgow, UK and with University of Surrey, UK (e-mail: m.imran@surrey.ac.uk).

Index Terms

Intensity modulation, Direct detection, unipolar transmission, orthogonal frequency division multi-
plexing, visible light communication.

I. INTRODUCTION

The emergence of visible light communication (VLC) technology has only been possible
via advances in and availability of cost-efficient light emitting diodes (LEDs), better known as
off-the-shelf LEDs. However, employing these LEDs as transmitters in VLC systems poses a
unique technical challenge at the receiver to extract the phase of the electrical sub-carrier from
the optical carrier [1]–[15]. This restriction limits the types of transceivers that can be used in
VLC systems; the common one being the intensity modulation/direct detection (IM/DD) type
of transceiver. Adding to that, the IM/DD channel in VLC systems further limits the transmit
signal to be non-negative, making the design of the electrical sub-carrier more challenging.

An adverse consequence of the above mentioned technical restrictions is the dramatic decrease
in efficiency of the legacy radio frequency (RF)-orthogonal frequency division multiplexing
(OFDM) method when it is directly applied to VLC [7], [16]. This explains the continuous effort
that has recently been put to adapt the legacy RF-OFDM method to VLC by converting its two-
dimensional (2D) time-domain signal into a one-dimensional unipolar signal [4]. To this end,
optical-OFDM (O-OFDM), which utilizes Hermitian symmetry prior to the inverse fast Fourier
transform (IFFT) operation, has been widely adopted in VLC since it allows to generate bipolar-
real-valued samples, and therefore, is compatible with LED transmission. Although O-OFDM
is very popular in VLC systems, it suffers from power inefficiency when it is compared to the
conventional coherent techniques where two bipolar carrier signals are individually modulated.
The power inefficiency is due to direct current (DC) shift that is required to convert its bipolar
O-OFDM signal into a non-negative signal. The aforementioned technique is known as direct-
current O-OFDM (DCO-OFDM) [1], [17] and it has been shown in the literature to require a

high DC-shift (i.e., leading to low power efficiency (PE) performance) to convert the bipolar into a unipolar signal [4]. Indubitably, the DC-shift process is a considerable waste of energy since it increases the necessary amount of transmit power. In turn, this severely affects the BER performance of such a system.

To improve the PE of DCO-OFDM, asymmetrically clipped O-OFDM (ACO-OFDM) has been proposed in the literature to generate a genuine unipolar signal over the IM/DD channel. In ACO-OFDM, a unipolar signal is produced by using the O-OFDM operation, but where only the odd subcarriers of the N-point IFFT are modulated, followed by clipping the negative time-domain O-OFDM samples to obtain a non-negative signal. Transmitting only over the odd subcarriers obviously reduces the spectral efficiency (SE) by a factor of two when compared to DCO-OFDM, which eliminates any PE benefits for high constellation sizes; whereas the clipping process leads to an additional 3 dB signal-to-noise ratio (SNR) penalty since it generates inter-modulation distortion. In order to enhance the SE of ACO-OFDM, the authors of [15] proposed the pulse-amplitude-modulated discrete multitone modulation (PAM-DMT) technique, which modulates only the imaginary part of the O-OFDM subcarriers to generate asymmetrically clipped non-negative signal, but without enhancing the error rate performance degradation in ACO-OFDM. A straightforward alternative to ACO-OFDM, known as unipolar-OFDM (U-OFDM)/Flip-OFDM, was proposed in [18], [19] by rearranging the bipolar O-OFDM samples such that the positive and negative samples of the O-OFDM time-domain signal are consecutively transmitted. This scheme is shown to be an effective solution for providing better error rate performance than ACO-OFDM when advanced detection techniques are employed. Unfortunately, U-OFDM/Flip-OFDM is inefficient for high-data-rate applications because of its inherent latency, which is twice as high as that of ACO-OFDM.

Designing an OFDM based scheme that is both SE (as DCO-OFDM) and PE (as ACO-OFDM) has proved difficult in the early development stage of VLC; however, two main tracks of research have recently been followed to achieve this goal. One research track focuses on

simultaneously transmitting an ACO-OFDM frame with a different unipolar OFDM-based frame over nonoverlapping frequency bands. Some of these techniques are asymmetrically clipped DC biased O-OFDM (ADO-OFDM) [20], [21], enhanced asymmetrically clipped DC biased O-OFDM (EADO-OFDM) [22], hybrid asymmetrically clipped OFDM (HACO-OFDM) [23] and asymmetrically and symmetrically clipped O-OFDM (ASCO-OFDM) [24], where ACO-OFDM is frequency division multiplexed with DCO-OFDM, DCO-OFDM, PAM-DMT or U-OFDM/Flip-OFDM), respectively. The other main research track focuses on combining several information streams of the same unipolar OFDM scheme [25]. In this context, there is an ever-growing list of variants of the ACO-OFDM and U-OFDM/Flip-OFDM techniques such as layered ACO-OFDM/spectral and energy efficient OFDM (SEE-OFDM) [26], [27]/enhanced ACO-OFDM [28], enhanced U-OFDM (eU-OFDM) [29], and recently the GREENER-OFDM scheme [30]. However, the main disadvantage of all these schemes (in both research tracks) is that system performance improvement is obtained at the cost of higher transceiver complexity (high computational complexity (CC) and memory requirements), which is at odds with the low-complexity philosophy of the IM/DD transmission scheme in VLC. For instance, a major drawback of GREENER-OFDM is that it requires a significant amount of memory at the transmitter side to generate one OFDM frame, which is formed by superimposing multiple streams of at least three streams of U-OFDM waveforms. Whereas, at the receiver side, an intensive high CC detection scheme (i.e., a successive interference cancellation (SIC) type of detector) is utilized to decode the information streams. Although GREENER-OFDM is able to achieve promising performance improvements, it entails high memory and large hardware resource utilizations, as well as a prohibitive CC compared with classic O-OFDM-based schemes, which makes it less practical and viable for VLC systems.

In this paper, we propose a new unipolar transmission scheme for VLC by following a new direction (i.e., by using orthogonal waveforms (OWs)) for converting the bipolar O-OFDM samples into a unipolar signal, and thus it can fit the IM/DD channel constraints without signal

clipping or DC-biasing, which is unlike that has so far been proposed in the literature. Thus the main contributions of this paper are:

- A new low-complexity unipolar transmission scheme, which we refer to as unipolar orthogonal transmission (UOT), is proposed for VLC systems; our scheme dose not require any DC-shift and/or clipping processes and thus, it is more reliable than ACO-OFDM. Moreover, by avoiding multi-layered signal transmission/reception in comparison with superimposed transmission schemes such as eU-OFDM or GREENER-OFDM and by using simple and robust transmission and detection techniques, it ensures that our scheme is practical with a low implementation complexity. This is unlike some of the most recently proposed techniques in the literature.

- The derivation of the analytical BER expression for our proposed UOT/UOT scheme (in the form of a compact computable formula) is provided; its great accuracy is verified through Monte Carlo simulations.

- A comprehensive performance analysis of our UOT scheme is performed; we present its performance and draw insights from it by comparing our scheme with the most widely investigated OFDM-based systems in VLC; i.e., DCO-OFDM and ACO-OFDM, in terms of both theoretical and practical key performance indicators, including error rate performance, SE, PE, peak to average power ratio (PAPR), inter-channel interference (ICI) and complexity. Note here that DCO-OFDM and ACO-OFDM are the two most pertinent schemes to compare our UOT scheme against given that, unlike most of the rest of the relevant schemes in the literature, our scheme relies on the same simple standard OFDM transceiver as these two schemes and its latency is almost similar to these schemes.

The paper is organized as follows. Section II describes the proposed system framework i.e. the considered channel model, a complete description of the system model and provides details regarding the design of our proposed UOT scheme by discussing both its transmitter and receiver

processes. In Section III, we derive the analytical BER of our UOT scheme and validate its accuracy via simulation. Section IV demonstrates the performance gains attained by our proposed scheme in comparison with relevant schemes in the literature, for instance, our scheme can achieve 3 dB SNR gain over ACO-OFDM, for the same SE. Section IV also presents practical performance analysis of our proposed scheme, including PAPR, complexity and the effect of miss-synchronization on its performance. Finally, conclusions are drawn in Section V.

II. SYSTEM MODEL

In a classic point-to-point VLC system, as it is shown in Fig. 1, transmission of data is performed by converting an electrical signal into an optical signal. The received signal $y(t)$ (i.e., the received photocurrent by the photodetector (PD)), can usually be expressed as

$$y(t) = \gamma \alpha h s(t) + \mathrm{z}(t) \tag{1}$$

where α is the electro-optical conversion factor in watts per ampere, γ reflects the photodetector responsivity, and $s(t)$ denotes the intensity modulated signal sent by the LED; due to the IM/DD channel practical constraint, $s(t)$ has to be a non-negative (i.e. unipolar) real valued signal, which fundamentally differentiates VLC signals from other signals used in wireless communication systems. Furthermore, the average transmitted optical power, i.e.

$$P_o = \lim_{T=\infty} \frac{\alpha}{T} \int_{-T}^{T} s(t) dt, \tag{2}$$

is limited to meet "eye safety" requirements. In addition, $\mathrm{z}(t)$ in (1) is the sum of the ambient shot
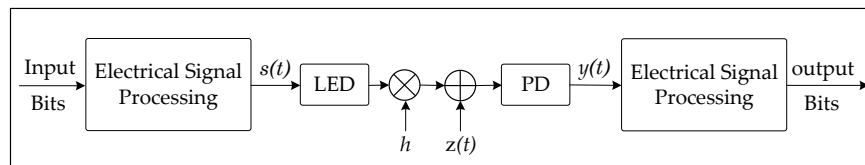

Fig. 1.   Generic model of a standard VLC system.

light noise and thermal noise, which is modelled as an additive white Gaussian noise (AWGN) with zero mean and variance σ^2 [31] and h represents the channel impulse response; here, h is the impulse response of the LED's light emission that is Lambertian in nature according to [32]. As it is depicted in Fig. 2, Lambertian emission can be modeled as a direct LOS DC gain such that [32], [33]

$$
h = \begin{cases} \dfrac{w^2 A}{d^2 \sin^2(\psi_c)} R_o(\phi) \cos(\psi), & 0 \le \psi \le \psi_c \\[2ex] 0, & \psi_c < \psi, \end{cases}
$$

where A is the detector area, w is the refractive index, d is the distance between the LED and PD, ϕ and ψ are the irradiance and incidence angles, respectively, and ψ_c is the field of view (FOV) semi-angle of the PD. In addition, the channel DC gain, $R_o(\phi) = [(\mathtt{m} + 1)/2\pi] \cos^{\mathtt{m}}(\phi)$, where $\mathtt{m} = -\ln(2)/\ln(\cos \phi_{1/2})$, and it denotes the order of the Lambertian emission; here, $\phi_{1/2}$ represents the transmitter semi-angle and $\ln(\cdot)$ is logarithm to base e.
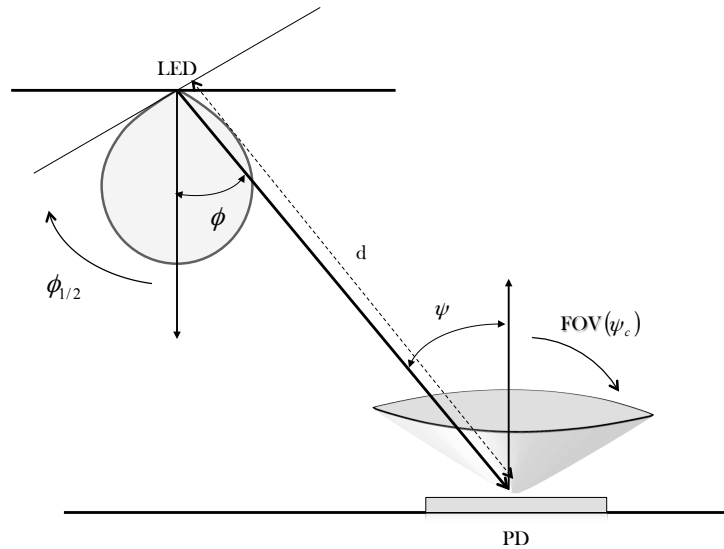

Fig. 2. Geometric representation of the line-of-sight (LOS) propagation model.

A. Transmitter Process

In our proposed method for unipolar transmission, the incoming bits $b \in \{0, 1\}$ are first mapped at the transmitter side to digital quadrature amplitude modulation (M-QAM) symbols $\ddot{s}_m$, $m \in \mathcal{M} = \{1, 2, \ldots, M\}$, where M is the constellation size of the M-QAM modulation. Because $s(t)$ in (1) must be a real valued signal, UOT employs an O-OFDM operation, which only modulates the odd subcarriers, as well as utilizes Hermitian symmetry in conjunction with IFFT. Thus, the $N = 4K$ input symbol frame of the IFFT is created from the K information symbols $\ddot{s}_m(k)$ by using the following symmetry property

$$\ddot{s}_m(2k-1) = \ddot{s}_m^\dagger(N - 2k + 1), \qquad k = 1, 2, \ldots, K;$$

$$\ddot{s}_m(2n) = 0, \qquad\qquad n = 0, 1, 2, \ldots, N/2 - 1,$$

where $[\cdot]^\dagger$ denotes the complex conjugate. Then the $N/2$ real valued sequence $\dot{s}(n)$ ($\forall n \in \mathcal{N} = \{0, 2, \ldots, N/2 - 1\}$) is obtained by feeding the frame of N symbols $\ddot{s}_m(n)$ to an IFFT operator; i.e.,

$$
\begin{bmatrix} \dot{s}(0) \\ \dot{s}(1) \\ \vdots \\ \dot{s}(N/2-1) \end{bmatrix} = \begin{bmatrix} 1 & 1 & \ldots & 1 \\ 1 & W_N & \ldots & W_N^{(N-1)} \\ \vdots & \vdots & \ldots & \vdots \\ 1 & W_N^{(N/2-1)} & \ldots & W_N^{(N/2-1)(N-1)} \end{bmatrix} \begin{bmatrix} 0 \\ \ddot{s}_m(1) \\ \vdots \\ \ddot{s}_m^\dagger(1) \end{bmatrix}, \tag{3}
$$

where $W_N = \exp(j2\pi/N)$. The analog transmitted signal $s(t)$ is then obtained by feeding the $N/2$ digital samples $\dot{s}(n)$ in (3) to a 2D digital converter as it is illustrated in Fig. 3, where each sample $\dot{s}(n)$ is mapped into a 2D point $\mathbf{s}(n) = [s_1(n), s_2(n)]$, based on the following mapping rule

$$\dot{s}(n) \geq 0 \Rightarrow s_1(n) = \dot{s}(n) \text{ and } s_2(n) = 0;$$
$$\dot{s}(n) < 0 \Rightarrow s_l(n) = -\frac{\dot{s}(n)}{\sqrt{2}}, \forall l \in \mathcal{L} = \{1, 2\}. \tag{4}$$

In other words, the bipolar digital sample $\dot{s}(n)$ is mapped into $\mathbf{s}(n) = [\dot{s}(n), 0]$, if it is positive, and into $\mathbf{s}(n) = -[\dot{s}(n), \dot{s}(n)]/\sqrt{2}$, if it is negative. Afterward, a pulse shaping operation is

performed and the continuous-time signal $s(t)$, which is then directly intensity modulated at the LED, can be expressed as $s(t) = s_1 p_1(t) + s_2 p_2(t)$, where $p_l(t)$ ($\forall l \in \mathcal{L}$) are two OWs that satisfy the following conditions

$$
\begin{aligned}
p_1(t) &\geq 0, &&\forall t \in \mathbb{R}; \\
p_1(t) + p_2(t) &\geq 0, &&\forall t \in \mathbb{R}; \\
\int_{-\infty}^{\infty} p_1(t)p_2(t)\, dt &= 0.
\end{aligned}
\tag{5}
$$

The list of conditions can be interpreted as: the system utilizes two non-negative unipolar waveforms where the first is a non-negative unipolar pulse $p_1(t)$, and the second is a non-negative unipolar pulse that is based on a combination of $p_1(t)$ and $p_2(t)$; this combination provides a second non-negative unipolar pulse shape for our proposed UOT scheme. Moreover, $p_1(t)$ and $p_2(t)$ are orthogonal to each others. Obviously, the selected pulse shapes; i.e., $p_1(t)$ and $p_2(t)$, that satisfy the conditions in (5) can transform any positive ($\dot{s}(n) > 0$) or negative ($\dot{s}(n) < 0$) real digital sample $\dot{s}(n)$ into a non-negative continuous-time waveform since according to (5), the impulse response of both $p_1(t)$ and the linear combination of $p_1(t)$ and $p_2(t)$ are always non-negative. An example of two pulse shapes that satisfy the conditions in (5) are the zero and the first order Walsh functions (rectangular waveforms) that are shown in Fig. 4. It should be noted here that the zero and the second order waveforms of the modified Hermite pulse and prolate spheroidal pulse sets also satisfy the conditions in (5); however, for the simplicity of introduction and fairness of comparison between the different schemes we only consider the
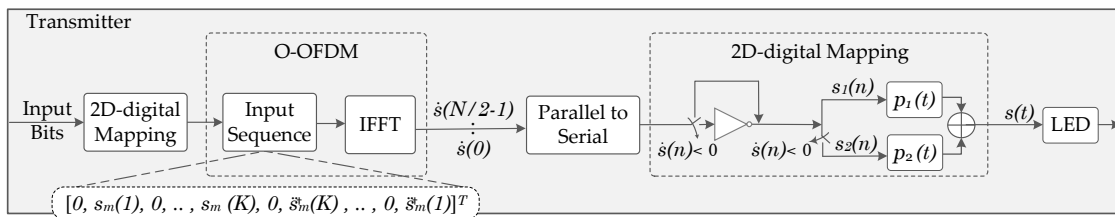

Fig. 3. Block diagram of our proposed UOT transmitter.

rectangular waveforms in the following. It should be noted here that unlike for an RF OFDM symbol, bandwidth (BW) constraints are not as critical in this system. As such, a sample-and-hold mechanism may be used in our scheme to convert the digital signal to analog signal [34].

In order to better understand how the transmit signal is generated in our scheme and how it differs from conventional unipolar schemes such as ACO-OFDM signal, Fig. 5 depicts both signals based on the same O-OFDM samples. First, note that the special arrangement in (3) helps to generate an output IFFT frame with an asymmetrical structure; i.e., the first $N/2$ samples at the output of the O-OFDM operation are repeated in the second half of the frame but with a reverse
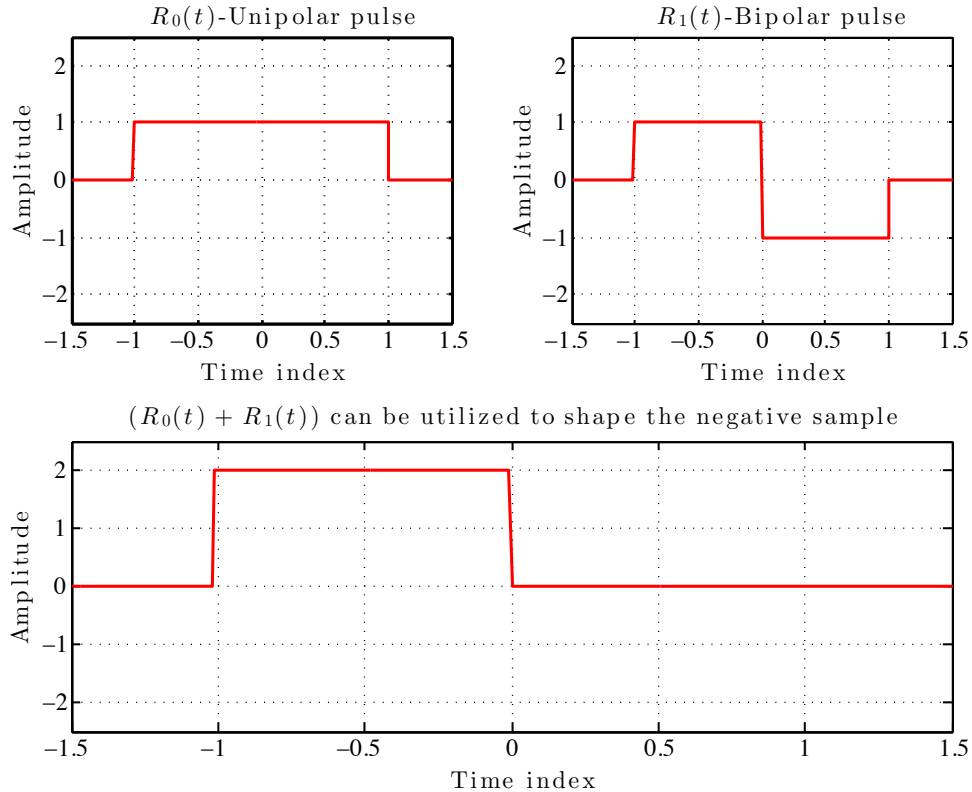

Fig. 4.   Normalized time response of the zero and first order Walsh rectangular orthogonal waveforms; i.e., $R_0(t)$ and $R_1(t)$, respectively, as well as the sum of these waveforms.

polarity [17], [21], [35]. Thus, unlike ACO-OFDM, our scheme does not require to convert the entire real-valued sequence of the O-OFDM operation since due to the anti-symmetry property of the time-domain samples, the first $N/2$ samples, i.e., $\dot{s}(n)$ ($\forall n \in \mathcal{N}$), would be sufficient at the receiver to recover the entire O-OFDM without any loss of information. It can be also seen in Fig. 5 (c), which shows an example of an analog signal generated by using our proposed UOT scheme (when using the zero and first order Walsh rectangular orthogonal waveforms) after the analog-to-digital converter (ADC), that the equivalent waveform duration of each sample in our
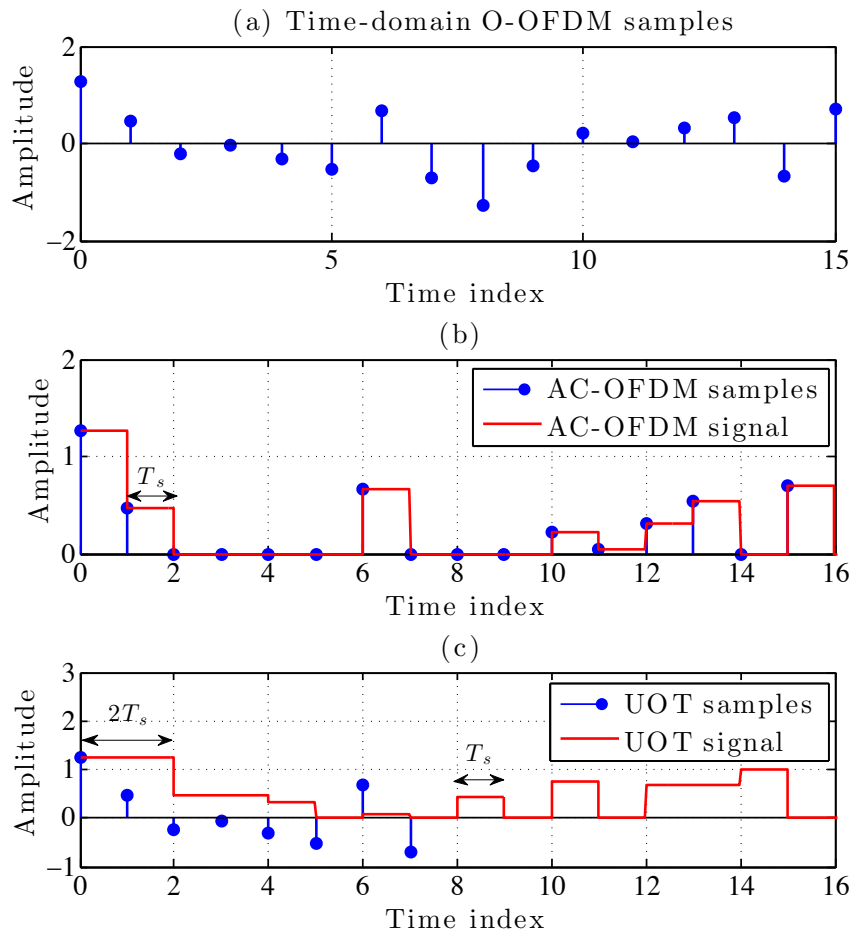

Fig. 5. Illustration of (a) time-domain O-OFDM sample; (b) an ACO-OFDM waveform and its time-domain samples based on the O-OFDM process of (a); (c) an UOT waveform and its time-domain samples based on the O-OFDM process of (a).

scheme can be expressed by

$$
s(t) = \begin{cases} \dot{s}(n)[u(t) - u(t - 2T_s)]/\sqrt{2}, & \dot{s}(n) \geq 0; \\[2mm] -\dot{s}(n)[u(t) - u(t - T_s)], & \dot{s}(n) < 0, \end{cases} \tag{6}
$$

where $u(\cdot)$ is the unit step function. Thus, the minimum pulse duration of our proposed UOT scheme T_s and the signal duration (the OFDM sampling period) of our proposed UOT scheme is $T = NT_s$, as in ACO-OFDM. Therefore, Fig. 5 and equation (6) indicate that our proposed UOT scheme has the same throughput and BW requirement as ACO-OFDM (i.e., our proposed UOT achieves the same SE when compared to ACO-OFDM).

B. Receiver process

In our proposed UOT scheme, upon reception of the transmitted waveform $s(t)$ over the AWGN channel, the received signal $y(t)$ is passed through two matched filters $\bar{p}_l = p_l(2T_s - t)$ ($\forall l \in \mathcal{L}$). After which the observations $\tilde{s}_l(n)$ ($\forall l \in \mathcal{L}$) are obtained. It should be noted here that since the sampling time is $2T_s$ there is no cross-channel interference between consecutive positive and negative samples at the sampling instance $2T_s$, as it is shown in Fig. 6. Note also that despite the fact that the transmitted signals in our proposed scheme are positive unipolar, the received samples $\bar{s}_l(n)$ ($\forall l \in \mathcal{L}$) are not necessary positive since the AWGN can be negative [36], [37]. Therefore, it has been proposed in the literature to clip the negative samples at the receiver (as a first stage) to force the negative samples to be equal to zero. This technique, which was utilized for ACO-OFDM in [34], can also be utilized in our proposed UOT scheme as an initial stage for noise clipping. Therefore, for the sake of completeness, we design here two detectors including or not the negative clipper, and assess their performance later in this paper. In the case that a negative clipper is not included, the receiver directly passes the received samples $\bar{s}_l(n)$ ($\forall l \in \mathcal{L}$) to detect the transmitted signals. Whereas if a negative clipper is included; the receiver first clips the negative observations before estimating the transmitted signal. Afterwards,
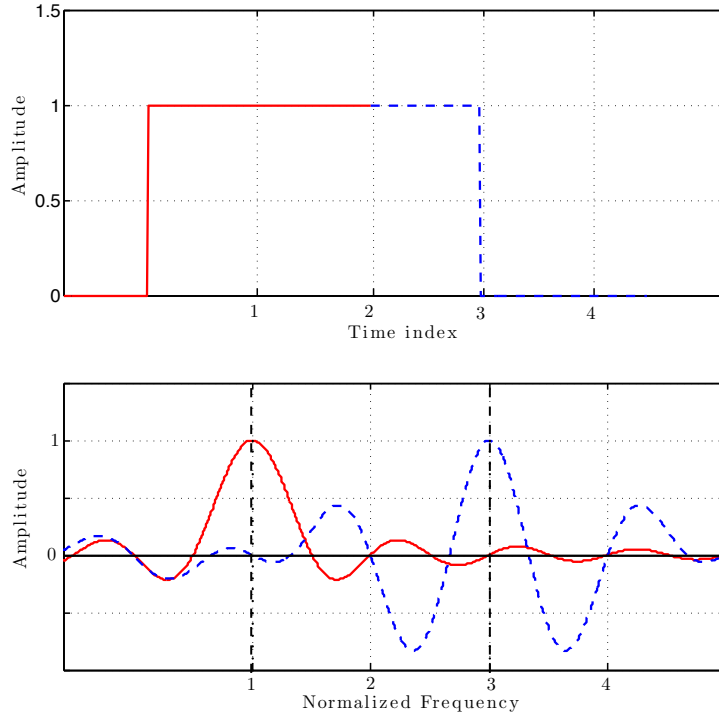
Fig. 6. Illustration of (a) time domain waveforms of positive (red solid line) and negative (blue dashed line) samples; (b) respective spectrum of positive (red solid line) and negative (blue dashed line) samples.

the receiver utilizes the orthogonality between $p_1(t)$ and $p_2(t)$ to distinguish whether the positive or the negative signal was transmitted as follows

$$s^*(n) = \tilde{s}_1(n)(1-\mathtt{p}) - \frac{\mathtt{p}}{\sqrt{2}}(\tilde{s}_1(n) + \tilde{s}_2(n)) \tag{7}$$

where $\tilde{s}_l(n) \triangleq \bar{s}_l(n)$ if no negative clipping is utilized and $\tilde{s}_l(n) \triangleq \max[\bar{s}_l(n), 0]$ if negative clipping is utilized. Moreover, $\mathtt{p}$ is defined as

$$\mathtt{p} = \begin{cases} 0, & \text{if } [\tilde{s}_1(n) - \tilde{s}_2(n)] > \tilde{s}_2(n); \\ \\ 1, & \text{otherwise.} \end{cases} \tag{8}$$

Given that the received observations $\tilde{s}_l(n)$ $(\forall l \in \mathcal{L})$ cannot be directly utilized to detect the polarity of the transmitted sample $\dot{s}(n)$ (since the waveform $p_1(t)$ is utilized for transmitting

both positive and negative sample $s(n)$), the metric in (8) is required to detect the polarity of the transmitted sample. Following the amplitude extraction in (7), the demodulation of our UOT signal may be accomplished by means of an N or $2N$-point standard FFT process to recover the bit stream. In the case that an N-FFT demodulator is used, the time separation between the $N/2$ recovered samples $s^*(n)$ ($\forall l \in \mathcal{L}$) is first set to T_s before reconstructing the entire O-OFDM frame as

$$s^*(0), \ldots, s^*(N/2 - 1), -s^*(0), \ldots, -s^*(N/2 - 1), \tag{9}$$

so that the period of the recovered UOT frame is $T = NT_s$. Whereas, in the case that a $2N$-point standard FFT process is considered, zeros are inserted between detected samples before reconstructing the entire O-OFDM frame as

$$s^*(0), 0, s^*(1), \ldots, s^*(N/2 - 1), -s^*(0), 0, -s^*(1), \ldots, -s^*(N/2 - 1), \tag{10}$$

so that the period of the recovered UOT frame is $2T = 2NT_s$. Note that for both cases the input-output relationship of our proposed UOT scheme can be expressed by

$$
\begin{bmatrix} S^*(0) \\ S^*(1) \\ \vdots \\ S^*(N-1) \end{bmatrix} =
\begin{bmatrix} f_0 & f_0 & \ldots & f_0 \\ f_1 & f_1 W_N^{-1} & \ldots & f_1 W_N^{-(N-1)} \\ \vdots & \vdots & \ldots & \vdots \\ f_{N-1} & f_{N-1} W_N^{-(N-1)} & \ldots & f_{N-1} W_N^{-(N-1)^2} \end{bmatrix}
\begin{bmatrix} 1 & 1 & \ldots & 1 \\ 1 & W_N & \ldots & W_N^{(N-1)} \\ \vdots & \vdots & \ldots & \vdots \\ 1 & W_N^{(N-1)} & \ldots & W_N^{(N-1)^2} \end{bmatrix}
\begin{bmatrix} 0 \\ \ddot{\mathbf{s}}_m(1) \\ \vdots \\ \ddot{\mathbf{s}}_m^\dagger(1) \end{bmatrix}
$$
$$
+ \begin{bmatrix} Z(0) \\ Z(1) \\ \vdots \\ Z(N-1) \end{bmatrix} \tag{11}
$$

which results in

$$
\begin{bmatrix} S^*(0) \\ S^*(1) \\ \vdots \\ S^*(N-1) \end{bmatrix} = \begin{bmatrix} f_0 & 0 & \dots & 0 \\ 0 & f_1 & \dots & 0 \\ \vdots & \vdots & \dots & \vdots \\ 0 & 0 & \dots & f_{N-1} \end{bmatrix} \begin{bmatrix} 0 \\ \ddot{\mathbf{s}}_m(1) \\ \vdots \\ \ddot{\mathbf{s}}_m^\dagger(1) \end{bmatrix} + \begin{bmatrix} Z(0) \\ Z(1) \\ \vdots \\ Z(N-1) \end{bmatrix} \tag{12}
$$

where

$$
f_n = \begin{cases} 1, & \text{if } s^*(n) \text{ is correctly detected;} \\ \\ -1/\sqrt{(2)}, & \text{otherwise.} \end{cases} \tag{13}
$$

Also, $Z(n)$ ($\forall n = \{1, 2, \dots, N\}$) are the noise components at the output of the IFFT. Note in (13) that $f_n \neq 0$, which is unlike the noise filtering algorithms proposed in [19], [38], and in turn the nonlinear detection operation in (7) do not lead to a loss of subcarrier orthogonality or ICI.

III. BER Performance Analysis

This section derives the BER of our proposed UOT transceiver on the premise that the communication channel is an AWGN and without considering the negative clipping. Accordingly, the error rate probability of our proposed transceiver can be evaluated by taking into account that the detection of $\dot{s}(n)$ is performed in two stages; the first stage detects the polarity of the transmitted symbol by using the metric in (8). The second stage then estimates the amplitude of the transmitted sample, based on the result of the first stage, by using equation (7). Thus, the correct detection of each individual sample in the time-domain depends on the correct detection of $\mathbf{p}$ and s^*, which is a function of two independent and normally distributed random variables $\tilde{s}_l$ ($\forall l \in \mathcal{L}$), i.e., $\tilde{s}_l \sim f_{\tilde{s}_l}(\mathbf{s}, \mu_{\tilde{s}_l}, \sigma_{\tilde{s}_l})$ such that

$$
f_{\mathbf{x}}(\mathbf{s}; \mu_{\mathbf{x}}, \sigma_{\mathbf{x}}) = \frac{1}{\sqrt{2\pi\sigma_{\mathbf{x}}^2}} exp\left(\frac{-(\mathbf{s} - \mu_{\mathbf{x}})^2}{2\sigma_{\mathbf{x}}^2}\right),
$$

where $\mu_{\mathtt{x}}$ and $\sigma_{\mathtt{x}}$ are the mean and the standard deviation of the variable $\mathtt{x}$. Note that the mean of the distribution of each random variable (RV) (i.e., $\tilde{s}_l$) depends on whether the transmitted signal $\dot{s}(n)$ is non-negative or negative. As a side note, we omit the index n in the rest of the derivation for simplicity of notation.

Let us first assume that the transmitted signal $\dot{s}$ is non-negative. Then, the probability to obtain the correct value of $\mathtt{p}$ is equivalent to correctly estimate the event $2\tilde{s}_2 < \tilde{s}_1$, where the random variables $\tilde{s}_1$ and $2\tilde{s}_2$ have a mean value of $\dot{s}$ and 0, respectively. Consequently, the conditional probability $p(2\tilde{s}_2 < \tilde{s}_1 | \tilde{s}_1 = \mathtt{s}) = \Phi(\mathtt{s}/2\sigma_2)$, where $\Phi(\cdot)$ is the cumulative probability distribution function of the standard normal RV, is the probability of correctly obtaining $\mathtt{p}$ when the observation value $\tilde{s}_1$ takes the value $\mathtt{s}$. Thus, the probability to correctly obtain $\mathtt{p}$ when the transmitted signal is non-negative, $P_c^+(\mathtt{p})$, which equals the unconditional probability that $2\tilde{s}_2$ does not exceed $\tilde{s}_1$, is, based on the law of total probability, given by

$$P_c^+(\mathtt{p}) = \int_{-\infty}^{\infty} f_{\tilde{s}_1}(\mathtt{s}; s_1, \sigma_1)\Phi\left(\frac{\mathtt{s}}{2\sigma_2}\right) d\mathtt{s}.$$

$$= \Phi\left(\frac{2s_1}{\sqrt{7\sigma^2}}\right).$$

Meanwhile, due to the detection process at the reciever, the transmitted sample will be transformed to a new value at the receiver, i.e., s^*, which its noise component can be calculated by using

$$\sigma_c^+(\dot{s}) = \frac{\int_{-\infty}^{\infty} \mathtt{s}^2 f_{\tilde{s}_1}(\mathtt{s}; s_1, \sigma_1)\Phi\left(\frac{\mathtt{s}}{2\sigma_2}\right) d\mathtt{s}.}{P_c^+(\mathtt{p})} - \left(\mu_c^+(\dot{s})\right)^2, \tag{14}$$

where $\mu_c^+(\dot{s})$ can be found by

$$\mu_c^+(\dot{s}) = \frac{\int_{-\infty}^{\infty} \mathtt{s} f_{\tilde{s}_1}(\mathtt{s}; s_1, \sigma_1)\Phi\left(\frac{\mathtt{s}}{2\sigma_2}\right) d\mathtt{s}.}{P_c^+(\mathtt{p})}. \tag{15}$$

The same methodology can be applied to derive the noise component of the detected sample when the transmitted signal is negative and the value of $\mathtt{p}$ is correctly detected, $\sigma_c^-(\dot{s})$. However,

recall that in the case of transmitting a negative sample, the probability $P_c^-(\mathrm{p})$ is equivalent to correctly estimate the event $(\tilde{s}_1 - \tilde{s}_2) < \tilde{s}_2$, where $\tilde{s}_1 - \tilde{s}_2$ and $\tilde{s}_2$ have a mean value 0 and $s_2 = \dot{s}/\sqrt{2}$, respectively. Note also that the received sample is mapped to the signal $(\tilde{s}_1 + \tilde{s}_2)/\sqrt{2}$ according to the detection rule in (7). Therefore, after some mathematical manipulation, the value of $\sigma_c^-(\dot{s})$ can be estimated by

$$\sigma_c^-(\dot{s}) = \frac{\displaystyle\int_{-\infty}^{\infty} 2\mathbf{s}^2 f_{\tilde{s}_2}(\mathbf{s}; s_2, \sigma_2) \Phi\left(\frac{\mathbf{s}}{\sigma}\right) d\mathbf{s}.}{P_c^+(\mathrm{p})} - \left(\mu_e^-(\dot{s})\right)^2, \tag{16}$$

where

$$\mu_c^-(\dot{s}) = \frac{\displaystyle\int_{-\infty}^{\infty} -\sqrt{2}\mathbf{s} f_{\tilde{s}_2}(\mathbf{s}; s_2, \sigma_2) \Phi\left(\frac{\mathbf{s}}{\sigma}\right) d\mathbf{s}.}{P_c^+(\mathrm{p})}.$$

The variances in (14) and (16) are defined based on the polarity of the variable $\dot{s}$. Thus, the average of the variances in (14) and (16) over the entire frame can be evaluated by

$$\sigma_c = \int_0^{\infty} \sigma_c^+(\dot{s}) d\dot{s} + \int_{-\infty}^0 \sigma_c^-(\dot{s}) d\dot{s}.$$

Note that the noise components in (14) and (16) are assumed to be an AWGN due to the central limit theorem (CLT) and the flat channel assumption.

Next, we need to obtain $\sigma^+(\dot{s})$ and $\mu^+(\dot{s})$ as well as $\sigma^-(\dot{s})$ and $\mu^-(\dot{s})$ for the case that p is mis-detected. Obviously, the probability of incorrectly detecting p when the transmitted signal is non-negative and negative equals the conditional probability $p(2\tilde{s}_2 > \tilde{s}_1 | \tilde{s}_1 = \mathbf{s})$ and $p((\tilde{s}_1 - \tilde{s}_2 > \tilde{s}_2 | \tilde{s}_2 = \mathbf{s})$, respectively. Consequently, the probability of incorrectly detecting p when the transmitted signal is non-negative and negative equals $P_e^+(\mathrm{p}) = 1 - P_c^+(\mathrm{p})$ and $P_e^-(\mathrm{p}) = 1 - P_c^-(\mathrm{p})$, respectively. Therefore, the expressions in (14) and (15) can be re-evaluated for the case when p is mis-detected as follows

$$\sigma_e^+(\dot{s}) = \frac{\displaystyle\int_{-\infty}^{\infty} \mathbf{s}^2 f_{\tilde{s}_1}(\mathbf{s}; s_1, \sigma_1) Q\left(\frac{\mathbf{s}}{2\sigma_2}\right) d\mathbf{s}.}{P_e^+(\mathrm{p})} - \left(\mu_c^+(\dot{s})\right)^2. \tag{17}$$

where $Q(\cdot)$ is the Q-function and

$$\mu_e^+(\dot{s}) = \frac{\displaystyle\int_{-\infty}^{\infty} -\mathbf{s} f_{\tilde{s}_1}(\mathbf{s}; s_1, \sigma_1) Q\left(\frac{\mathbf{s}}{2\sigma_2}\right) d\mathbf{s}.}{P_e^+(\mathbf{p})}.$$

for the case when the transmitted signal is non-negative, $\dot{s} \geq 0$. Whereas when $\dot{s} < 0$ (16) and (17) can be re-expressed as

$$\sigma_e^-(\dot{s}) = \frac{\displaystyle\int_{-\infty}^{\infty} 2\mathbf{s}^2 f_{\tilde{s}_2}(\mathbf{s}; s_2, \sigma_2) Q\left(\frac{\mathbf{s}}{\sigma}\right) d\mathbf{s}.}{P_e^-(\mathbf{p})} - \left(\mu_e^-(\dot{s})\right)^2, \tag{18}$$

where

$$\mu_e^-(\dot{s}) = \frac{\displaystyle\int_{-\infty}^{\infty} \sqrt{2}\mathbf{s} f_{\tilde{s}_2}(\mathbf{s}; s_2, \sigma_2) Q\left(\frac{\mathbf{s}}{\sigma}\right) d\mathbf{s}.}{P_e^-(\mathbf{p})}.$$

Similar to (14) and (16), (17) and (18) are defined based on the polarity of the variable $\dot{s}$. Thus, the average of the variances in (17) and (18) over the entire frame can be evaluated by

$$\sigma_e = \int_0^\infty \sigma_e^+(\dot{s}) d\dot{s} + \int_{-\infty}^0 \sigma_e^-(\dot{s}) d\dot{s}.$$

We know from the Bussgang theorem [38] that if $P(x)$ is a nonlinear transformation of a zero mean Gaussian RV x, then $P(x) = \zeta x + z$, where $\mathrm{E}[xz] = 0$ and ζ is a constant. Consequently, ζ and z can be evaluated for both correct and incorrect cases by using

$$\zeta_d = \frac{\mathrm{E}[\dot{s}\mu_d(\dot{s})]}{\sigma_{\dot{s}}^2}$$

$$= \frac{1}{\sigma_{\dot{s}}^2}\left(\int_0^\infty \dot{s}\mu_d^+(\dot{s}) f_{\dot{s}}(\mathbf{s}; 0, \sigma_{\dot{s}}) d\dot{s} + \int_{-\infty}^0 \dot{s}\mu_d^-(\dot{s}) f_{\dot{s}}(\mathbf{s}; 0, \sigma_{\dot{s}}) d\dot{s}\right),$$

and

$$z_d = \int_0^\infty \left(\mu_d^+(\dot{s})\right)^2 f_{\dot{s}}(\mathbf{s}; 0, \sigma_{\dot{s}}) d\dot{s} + \int_{-\infty}^0 \left(\mu_d^-(\dot{s})\right)^2 f_{\dot{s}}(\mathbf{s}; 0, \sigma_{\dot{s}}) d\dot{s} - \zeta_d^2 \sigma_{\dot{s}}^2,$$

where $d = c$ and e for the cases of correct and incorrect detection, respectively. Hence, the average of the gain factor and the noise component, i.e. $\bar{\zeta}$ and $\bar{z}$, respectively can be calculated by using

$$\bar{\zeta} = P_c\zeta_c + (1 - P_c)\zeta_e, \tag{19}$$

and

$$\bar{z} = P_c(\sigma_c + z_c) + (1 - P_c)(\sigma_e + z_e), \tag{20}$$

where P_c is the average probability of correct detection that can be estimated by

$$P_c = \int_0^\infty \Phi\left(\sqrt{\frac{4\dot{s}^2}{7\sigma^2}}\right) f_{\dot{s}}(\mathbf{s}; 0, \sigma_{\dot{s}})d\dot{s} + \int_{-\infty}^0 \Phi\left(\sqrt{\frac{2\dot{s}^2}{5\sigma^2}}\right) f_{\dot{s}}(\mathbf{s}; 0, \sigma_{\dot{s}})d\dot{s}.$$

Finally, invoking (19) and (20) in the BER formula of the M-QAM, the BER performance of our proposed scheme can be expressed by

$$\text{BER}_{UOT} = \text{BER}_{QAM}\left(\frac{\bar{\zeta}\text{E}_b}{\bar{z}}\right). \tag{21}$$

where BER_{QAM} is the conventional BER expression of M-QAM and E_b is the electrical energy per bit.

Figure 7 illustrates a comparison between the numerical results of our derived BER expression provided in (21) and Monte Carlo simulations for our proposed UOT transceiver without negative clipping and different constellation sizes; $M = 16, 64$ and 256. The figure clearly shows that the simulations and analytical BER results are in-line with each other, which validates the great accuracy of our derived BER expression in (21). Whereas in Fig. 8 we compare the BER performance of our UOT scheme when negative clipping is used or not prior to the detection process. The results show that contrary to ACO-OFDM, the usage of negative clipping does not enhance the BER performance in our scheme, such that this process can be avoided to reduce its implementation complexity. This can be attributed to the fact that in our proposed scheme the received signal (and; thus, the channel noise variance σ^2) is split over two matched filters at the receiver, which improves its immunity to noise. This can also be explained by considering that

though recovering $s^*(n)$ from $\tilde{s}_l$ ($\forall l \in \mathcal{L}$) requires additional polarity information from p, and, thus, any incorrect flipped polarity due to the noise process will then lead to a corresponding error in $s^*(n)$ as well; this error propagation only occurs when the noise at the output of the second matched filter, $\bar{p}_2(t)$, is larger than the signal at the output of the first matched filter, $\bar{p}_1(t)$. Hence, errors are most likely to occur on those signal points with relatively low power. On the one hand, the incorrect polarity of low-power signals will only have a marginal effect on the results. On the other hand, it will be highly unlikely for a large-magnitude signal to have an incorrect polarity due to a very large noise [39]. Therefore, $s^*(n)$ is only likely to suffer from a small SNR penalty, and thus the performance of the system is not improved by using a negative
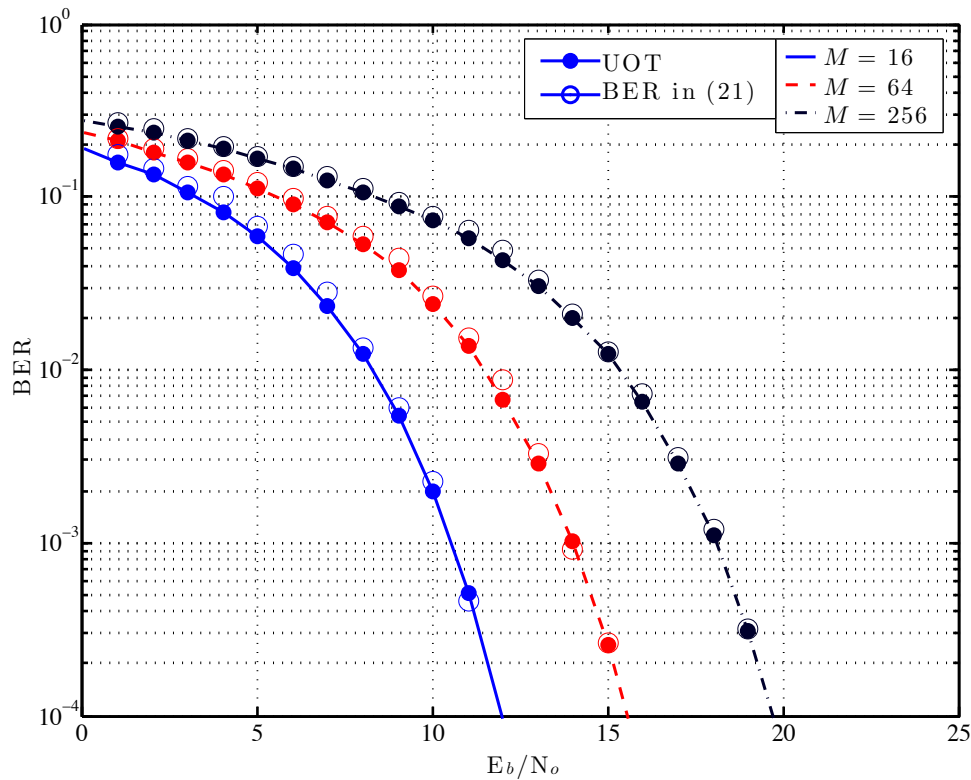

Fig. 7.   Comparison of the simulated (via Monte Carlo simulation) against the theoretical (via (21)) BER performance results of our proposed UOT scheme without negative clipping for various constellation sizes.

clipper at the receiver, as compared with conventional schemes such as ACO-OFDM.

IV. NUMERICAL RESULTS AND ANALYSIS

In this section, we first present numerical case studies on the error rate performance of our proposed UOT scheme and discuss its energy efficiency (EE) and SE in light of state-of-the-art schemes such as ACO-OFDM and DCO-OFDM. Also, in order to get insight into its performance, we then discuss how its design makes it efficient and robust in terms of practical considerations in comparison with the state-of-the-art. Furthermore, since practical IFFT/FFT sizes are greater than 64, in our simulations an IFFT/FFT size of 512 is chosen. Also, note that in general a carrier prefix (CP) is included in OFDM-based systems to combat inter-symbol
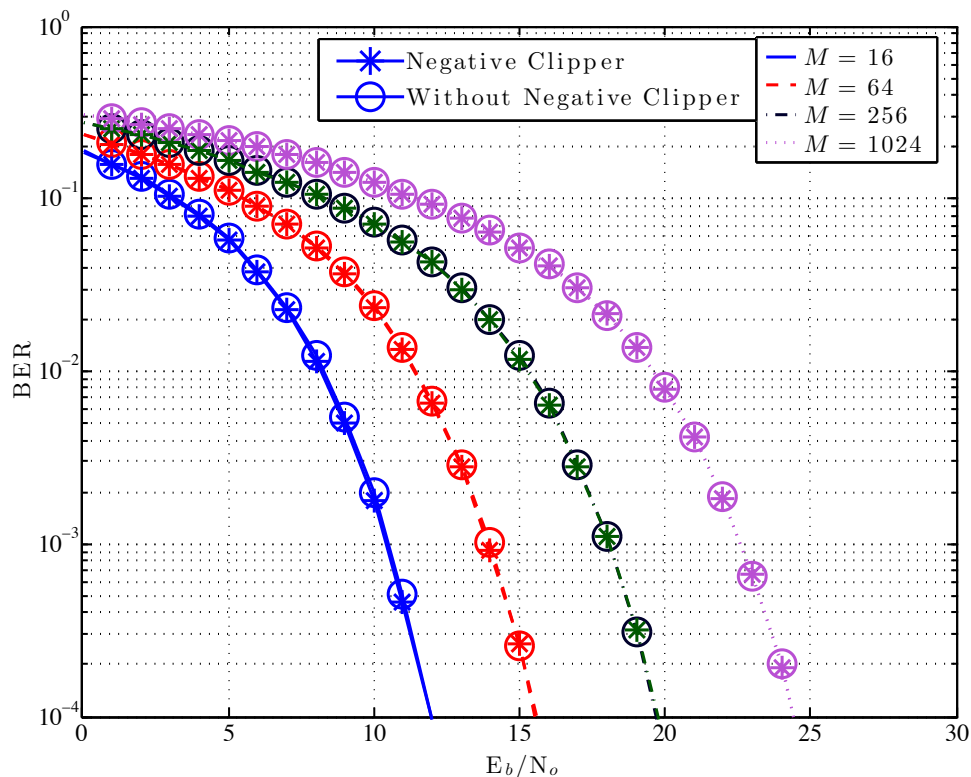

Fig. 8.   Effects of noise clipping on the BER performance of our UOT scheme at the receiver for different constellation sizes.

interference and ICI. However, in optical wireless systems the CP is shown to have a negligible impact on the electrical SNR requirement and SE [40]. Therefore, CP is not considered in our simulations. Furthermore, recall that link parameters such as the FOV, α, ϕ, $\phi_{1/2}$ and γ determine the optical path gain coefficient, h, which is merely a factor in the detection process, implying that a change in h would result in an equal SNR penalty for all the considered schemes in this section. Therefore, as in [14], we set $h = 1$ for simplicity reason.

A. EE and SE gains

Figure 9 assesses the BER performance of our proposed UOT in comparison with the state-of-the-art ACO-OFDM scheme for different constellation sizes. Recall that, as previously mentioned
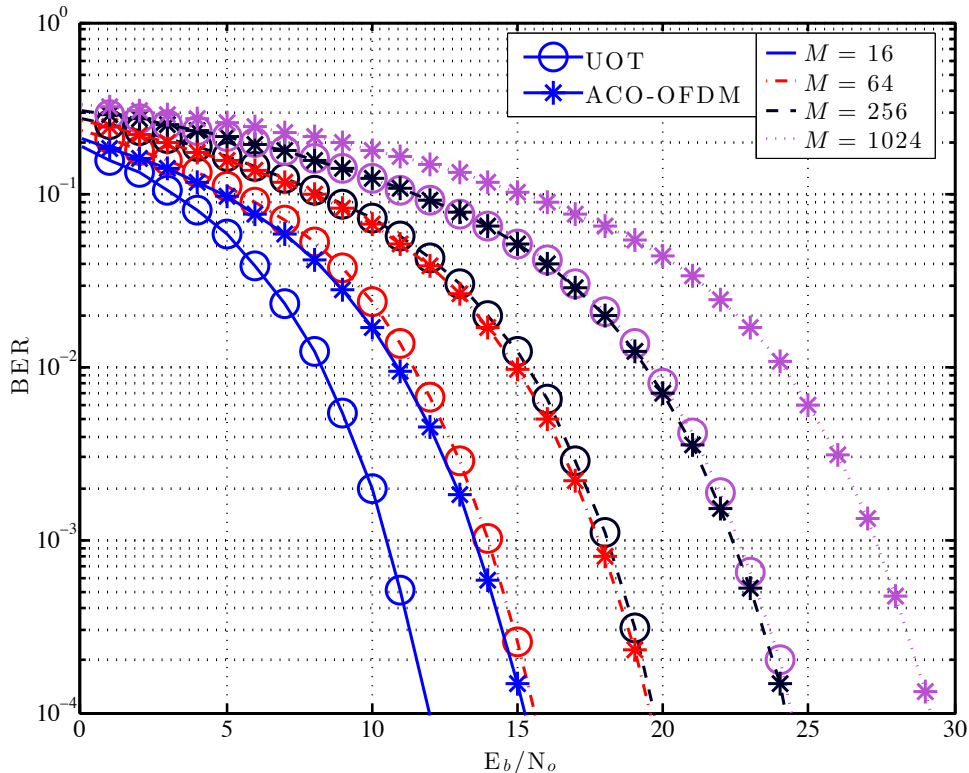

Fig. 9.   BER performance comparison of our proposed UOT scheme against ACO-OFDM for different constellation sizes.

the sampling time of UOT is twice as the one of ACO-OFDM such that both schemes are compared on equal ground in terms of SE. It can be observed in Fig. 9 that our proposed UOT scheme exhibits a very significant BER performance improvement as compared to ACO-OFDM. For instance, at a target BER performance of 10^{-4}, our proposed UOT scheme enhances the EE performance by almost 3 dB as compared to ACO-OFDM for $M = 16$, and this gain further increases as the constellation size, M, increases, i.e. a gain of 5 dB is achieved at a BER of 10^{-4} for $M = 1024$. This large performance gain is due to the fact that our proposed UOT scheme completely avoids clipping the negative samples (i.e., our proposed scheme exhibits no clipping noise on even sub-carriers); in turn, this implies a 3 dB enhancement at high E_b/N_0 in comparison with schemes using clipping like ACO-OFDM. Furthermore, the second step of our proposed detection method in (7) discards the second observation $\tilde{s}_2(n)$ for detecting the positive signal, which is only a noise component, and divides the noise component by $\sqrt{2}$ for detecting the negative signal; in turn, this improves the detection of the amplitude value of the recovered sample, and thus enhances the BER performance of our proposed UOT scheme over the conventional detection scheme in ACO-OFDM, as it is confirmed in Fig. 9.

In Fig. 10, our proposed scheme is compared against the state-of-the-art DCO-OFDM for different constellation sizes. It should be noted here that in order to circumvent the very high PAPR characteristic of the OFDM signal in DCO-OFDM, the DC shift is not necessarily evaluated based on the minimum peak of the transmitted signal for each constellation size; instead, it is first estimated based on simulations, it is then applied to the DCO-OFDM signal, and finally the remaining negative parts of the signals are clipped (after the DC-shift is applied) [29]. According to [29], the optimal DC shift values for constellation sizes $M = [16, 64, 256, 1024]$ are $[7, 9.5, 11, 13]$, respectively, in DCO-OFDM. Consequently, as in [29], we have used these values for simulating the BER performance of DCO-OFDM in Fig. 10. This figure illustrates that our proposed scheme can improve the EE by more than 2 dB at a BER of 10^{-4} in comparison to DCO-OFDM (when considering the same SE for both scheme); this can be observed by comparing

the result of our proposed UOT scheme for $M = 256$ against the result of DCO-OFDM for $M = 16$. It is intuitively clear that DCO-OFDM scheme has a SE of $\eta_{DC} = \log_2 M/2$ for a given constellation size M, whereas UOT has the same SE as ACO-OFDM, i.e. $\eta_{AC} = \log_2 M/4$, such that UOT with a constellation size of M^2 is equivalent to DCO-OFDM with a constellation size of M in terms of SE. Indeed, UOT with $M = 256$ (i.e. $\eta_{UOT} = \log_2 M/4 = 2$ bits/s/Hz when $M = 256$) produces the same SE as DCO-OFDM with $M = 16$ (i.e., $\eta_{DC} = \log_2 M/2 = 2$ bits/s/Hz when $M = 16$). The gain of our scheme over DCO-OFDM can be explained by noticing that our scheme electrical E$_b$/N$_o$ is almost similar to that of a bipolar OFDM signal, which is unlike ACO-OFDM. Whereas DCO-OFDM electrical E$_b$/N$_o$ is 6-7 dB worst that of a bipolar OFDM signal for a 4-QAM and this E$_b$/N$_o$ loss dramatically increases with the modulation order M. Consequently, our proposed scheme performs better than DCO-OFDM (as shown in Fig. 10) for constellation sizes higher than $M = 4$, which is unlike ACO-OFDM.

B. Practical issues

1) Optical power: The probability density function (PDF) distribution of the digital samples $\dot{s}(n)$ in our proposed UOT scheme is half normal-distribution, and, hence, can be expressed by [41]

$$f_{s(n)}(\mathbf{s}) = \frac{\sqrt{2}}{\sigma_{\dot{s}(n)}\sqrt{\pi}} e^{\left(\frac{-\mathbf{s}^2}{2\sigma_{\dot{s}(n)}^2}\right)} u(\mathbf{s}). \tag{22}$$

such that $\dot{s}(n)$ has an average optical power that is equal to

$$\mathrm{E}[\mathbf{s}(n)] = \int_{-\infty}^{\infty} \mathbf{s} f_{s(n)}(\mathbf{s}) d\mathbf{s} = \sqrt{\frac{2}{\pi}} \sigma_{\dot{s}(n)}. \tag{23}$$

However, extending the sampling time to $2T_s$ results in an average optical transmitted power that is $1/\sqrt{2}$ times the average optical power in (23) (i.e., $P_o = \mathrm{E}[\mathbf{s}(n)]/\sqrt{2}$) such that the average transmitted optical power of our UOT scheme is 40% higher than the average optical transmitted power by using ACO-OFDM.
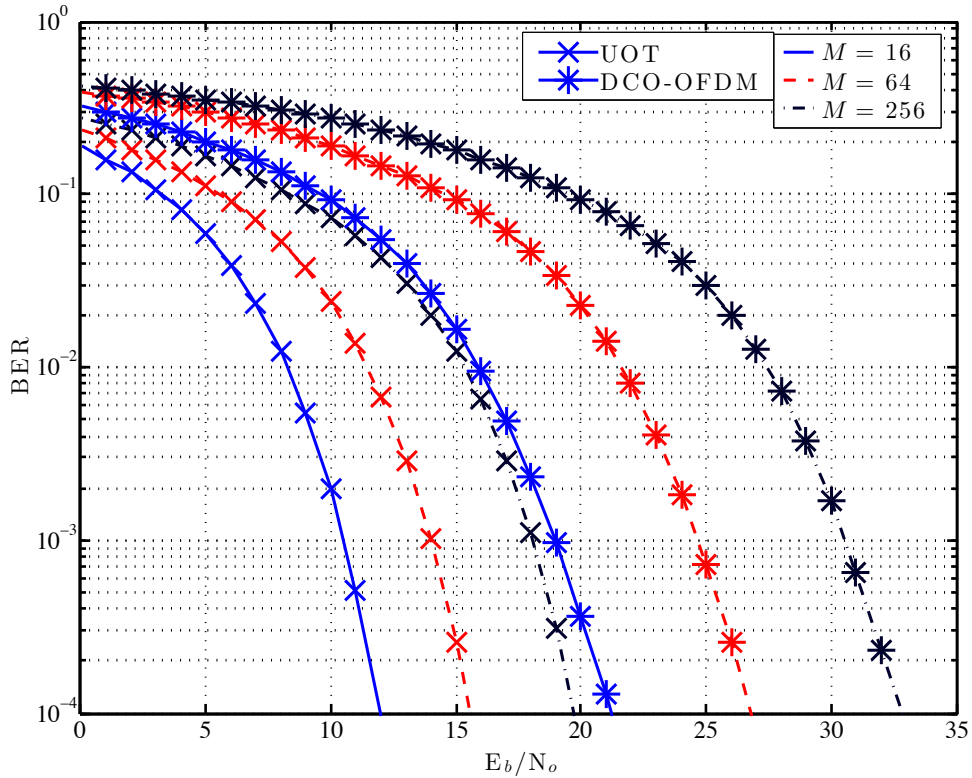
Fig. 10. BER performance comparison of our proposed UOT scheme against DCO-OFDM for different constellation sizes.

2) PAPR: The multi-carrier time-domain OFDM signal, as previously mentioned, is the result of the addition of a large number of sub-carriers, and, in turn it exhibits an inherently high PAPR. In VLC, LEDs have a limited operating voltage range and the voltage-current characteristic shows a nonlinear behavior. Thus, when an OFDM signal is used to intensity modulate LEDs, the high PAPR of the OFDM signal causes LED chip overheating and nonlinear distortions. Therefore, the PAPR of the output signal plays a vital role in determining the overall system practical performance and is considered as an essential performance metric.

The PAPR is defined as the ratio of peak signal power to average signal power. For OFDM-based systems, the PAPR is computed per OFDM frame and it is usually assessed in terms of the complimentary cumulative distribution function (CCDF), which is the probability that the

PAPR exceeds a certain value x, where the CCDF$= 1 - P(\text{PAPR} \leq x)$, and the PAPR of the continuous time output OFDM signal in decibels can be calculated by

$$\text{PAPR} = 10 \log_{10} \frac{\max[s^2(t)]}{\text{E}[s^2(t)]} \tag{24}$$

Using this metric, we assess, in Fig. 11, the PAPR performance of our UOT scheme against ACO-OFDM as a function of the threshold x. Results show that the PAPR performance of our proposed UOT scheme is similar to that of ACO-OFDM. This can be explained by considering that the PAPR of ACO-OFDM is twice as the one for O-OFDM. Indeed, in ACO-OFDM, the clipping of (on average) half the samples reduces the average energy of the signal, i.e. $E[s(t)^2]$, by half compared to O-OFDM; whereas $\max[s(t)^2]$ remains similar. Hence, based on (24), these PAPRs differ by a factor of two. Meanwhile, the PAPR of our UOT scheme is also twice as the one of
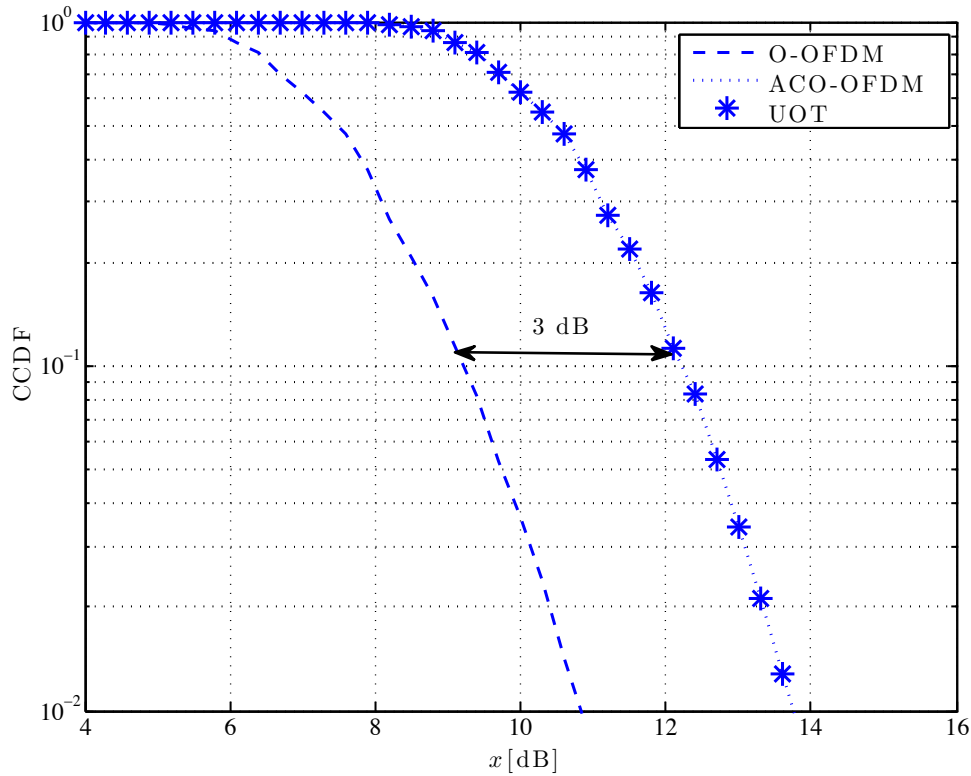

Fig. 11.   PAPR comparison between our proposed UOT scheme and ACO-OFDM for the same data information.

O-OFDM and, thus, similar to ACO-OFDM; the PAPR of the signal being inversely proportional to the duty cycle of the transmitting pulse, which in our proposed scheme is $(T_s/2)/T_s = 0.5$, implies that the PAPR of our UOT scheme is also twice that of O-OFDM.

3) Complexity: In terms of implementation complexity, our proposed UOT scheme employs at the transmitter side a simple sample and hold technique, which varies depending on the polarity of the transmitted signal. Whereas at the receiver side, it requires an additional filter to detect the polarity of the transmitted signal, in comparison with ACO-OFDM. However, in terms of CC, though our proposed scheme needs to recover two samples per transmitted waveform to decode each one of them, it requires a total of N samples to recover the entire O-OFDM frame, which is similar to ACO-OFDM. Obviously, the number of FFT/IFFT operations in both of the schemes is the same, and thus their CC is similar. Note that the additional step in (8) that recovers the polarity in our proposed UOT scheme has a complexity of one real addition, and; thus, it has a negligible effect on the CC.

4) Timing Jitter: Given that our proposed scheme detector employs two detection stages to estimate any transmitted symbol, it is relevant to investigate under which circumstances the system performance can be limited by the inherent timing jitter error. The first detection stage estimates the polarity of the transmitted signals, whereas the second stage determines the amplitude of the symbol based on the previous stage. However, the first stage relies on OWs, which is known to have a challenging autocorrelation characteristic; i.e., OWs exhibits time-sensitivity to receiver synchronization and clock sampling jitters. Adversely, in practical systems, the estimated sampling clock times at the receiver deviates from the ideal sampling time, which usually referred to as timing jitter, and causes BER performance losses. Figure 12 depicts the impact of timing jitter on the BER performance of our proposed scheme for different timing jitter; $\varepsilon = 0s, 0.01s, 0.03s \ldots, .23s$, where the jitter error is modeled as a positive and uniformly distributed random timing jitter in the range of $[0; \varepsilon]$ as in [42], for an M-QAM constellation. Clearly, the presence of synchronization jitter causes the matched filter to sample
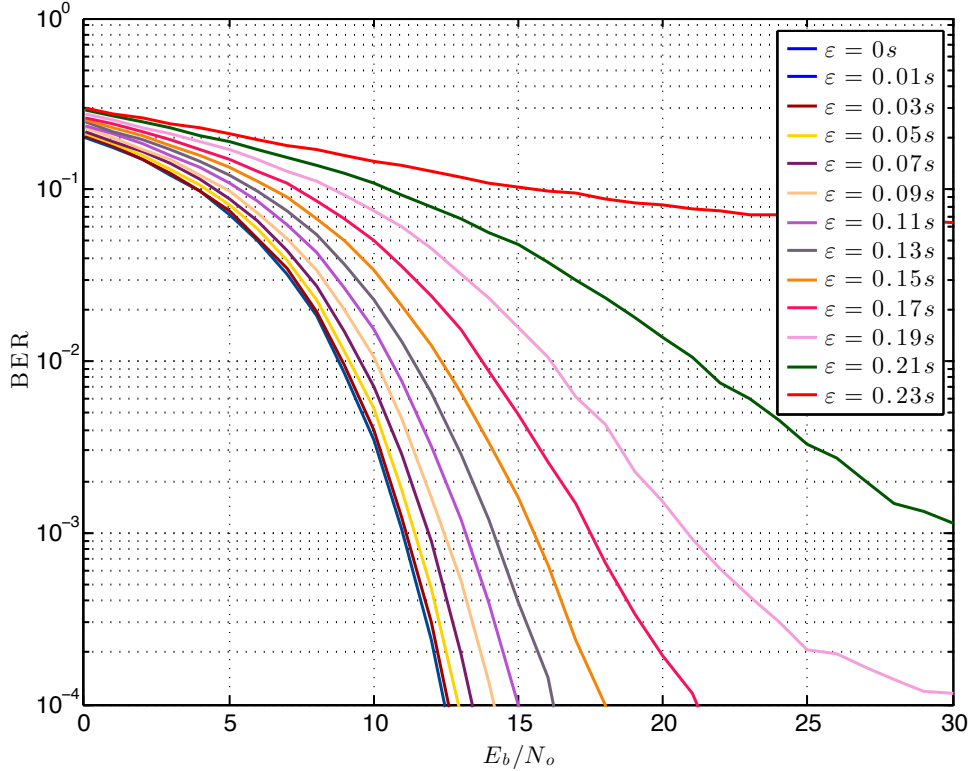
Fig. 12.   Effect of the timing jitter on our proposed UOT transceiver BER performance for a constellation size $M = 16$.

the received signal, not at the sampling instant $t = T_c$, but at random samples in its vicinity,

altering the detected two parts of **s** and degrading the BER performance of the system. It can be

observed in Fig. 12 that the timing jitter has a little effect on the preformance (less than 1 dB) for

timing offsets of less than 0.07. However, for higher timing offsets, additional power is required

to achieve specific BERs and this power increases exponentially as the timing jitter increases.

But note that the jitter noise plateau level of our proposed scheme occurs when $\varepsilon = 0.23$ which

indicates that our proposed UOT transceiver is a jitter-robust transceiver unlike other orthogonal

transmission schemes in the literature such as multilevel pulse position modulation [43].

V. CONCLUSION

This paper proposes a novel transceiver for VLC by relying on OWs to ensure the unipolarity of the transmit signal carrier, which is one of the major technical requirement for transmitting information over an IM/DD channels. More, precisely the scheme conveys the polarity of the bipolar symbol through the amplitudes and indices of the transmitted 2D OW, which is in a clear contrast with the existing approaches in the literature. An analytical derivation of the BER for our proposed scheme is presented, and its result matches the Monte Carlo BER simulation. Simulated results show that substantial performance gains in terms of BER that can be achieved by our proposed scheme when compared with its existing relevant counterparts at no expense in terms of SE, PAPR and complexity. The proposed scheme is also shown to be robust against timing jitter error and noise, which is distinctly novel in comparison with existing VLC systems.

REFERENCES

[1] S. Mazahir, A. Chaaban, H. Elgala, and M. Alouini, "Achievable rates of multi-carrier modulation schemes for bandlimited im/dd systems," *IEEE Trans. Wireless Commun.*, vol. 18, no. 3, pp. 1957–1973, Mar. 2019.

[2] X. Zhang, Z. Babar, R. Zhang, S. Chen, and L. Hanzo, "Multi-class coded layered asymmetrically clipped optical OFDM," *IEEE Trans. Commun.*, vol. 67, no. 1, pp. 578–589, Jan. 2019.

[3] Z. Babar, X. Zhang, P. Botsinis, D. Alanis, D. Chandra, S. X. Ng, and L. Hanzo, "Near-capacity multilayered code design for LACO-OFDM-Aided optical wireless systems," *IEEE Trans. Veh. Technol.*, vol. 68, no. 4, pp. 4051–4054, April 2019.

[4] J. Zhou and W. Zhang, "A comparative study of unipolar OFDM schemes in Gaussian optical intensity channel," *IEEE Trans. Commun.*, vol. 66, no. 4, pp. 1549–1564, April 2018.

[5] F. Wu, L. Chen, S. Cai, and W. Wang, "Experimental study and application of response mask invariant characteristic for generalized visible light communication channel," *IEEE Photon. J.*, vol. 10, no. 3, pp. 1–12, June 2018.

[6] R. Bai, Z. Wang, R. Jiang, and J. Cheng, "Interleaved DFT-spread layered/enhanced ACO-OFDM for intensity-modulated direct-detection systems," *J. Lightw. Technol.*, vol. 36, no. 20, pp. 4713–4722, Oct. 2018.

[7] D. W. Dawoud, F. Heliot, M. A. Imran, and R. Tafazolli, "A novel orthogonal transmission scheme for visible light communication," in *IEEE Int. Conf. Commun., (ICC), Kansas City, MO*, May 2018.

[8] F. Yang, Y. Sun, and J. Gao, "Adaptive LACO-OFDM with variable layer for visible light communication," *IEEE Photon. J.*, vol. 9, no. 6, pp. 1–8, Dec. 2017.

[9] A. Yesilkaya, E. Basar, F. Miramirkhani, E. Panayirci, M. Uysal, and H. Haas, "Optical MIMO-OFDM with generalized LED index modulation," *IEEE Trans. Commun.*, vol. 65, no. 8, pp. 3429–3441, Aug. 2017.

[10] B. Li, W. Xu, H. Zhang, C. Zhao, and L. Hanzo, "Papr reduction for hybrid aco-ofdm aided im/dd optical wireless vehicular communications," *IEEE Trans. Veh. Technol.*, vol. 66, no. 10, pp. 9561–9566, Oct. 2017.

[11] O. Narmanlioglu, R. C. Kizilirmak, and M. Uysal, "The impact of pulse shaping filters on OFDM-based visible light communications," in *Int. Conf. on Application of Info. and Commun. Techs.*, Oct 2016, pp. 1–4.

[12] F. Yang, J. Gao, and S. Liu, "Novel visible light communication approach based on hybrid OOK and ACO-OFDM," *IEEE Photon. Technol. Lett.*, vol. 28, no. 14, pp. 1585–1588, July 2016.

[13] M. Noshad and M. Brandt-Pearce, "Hadamard-coded modulation for visible light communications," *IEEE Trans. Commun.*, vol. 64, no. 3, pp. 1167–1175, Mar. 2016.

[14] S. Dimitrov, S. Sinanovic, and H. Haas, "Clipping noise in OFDM-based optical wireless communication systems," *IEEE Trans. Commun.*, vol. 60, no. 4, pp. 1072–1081, Apr. 2012.

[15] S. C. J. Lee, S. Randel, F. Breyer, and A. M. J. Koonen, "PAM-DMT for intensity-modulated and direct-detection optical communication systems," *IEEE Photon. Technol. Lett.*, vol. 21, no. 23, pp. 1749–1751, Dec 2009.

[16] D. W. Dawoud, F. Heliot, M. A. Imran, and R. Tafazolli, "Spatial quadrature modulation for visible light communication in indoor environment," in *IEEE Int. Conf. Commun., Paris, (ICC)*, May 2017.

[17] J. Armstrong and B. J. C. Schmidt, "Comparison of asymmetrically clipped optical OFDM and DC-biased optical OFDM in AWGN," *IEEE Commun. Lett.*, vol. 12, no. 5, pp. 343–345, 2008.

[18] D. Tsonev, S. Sinanović, and H. Haas, "Pulse shaping in unipolar OFDM-based Modulation Schemes OFDM-based communication system," no. 2, pp. 1208–1212, 2012.

[19] N. Fernando, Y. Hong, and E. Viterbo, "Flip-OFDM for unipolar communication systems," *IEEE Trans. Commun.*, vol. 60, no. 12, pp. 3726–3733, Dec. 2012.

[20] S. D. Dissanayake, K. Panta, and J. Armstrong, "A novel technique to simultaneously transmit ACO-OFDM and DCO-OFDM in IM/DD systems," in *IEEE GLOBECOM Wkshps*, Dec. 2011, pp. 782–786.

[21] S. D. Dissanayake and J. Armstrong, "Comparison of ACO-OFDM, DCO-OFDM and ADO-OFDM in IM/DD systems," *J. Lightw. Technol.*, vol. 31, no. 7, pp. 1063–1072, Apr. 2013.

[22] R. Bai, J. Chen, T. Mao, and Z. Wang, "Enhanced asymmetrically clipped DC biased optical OFDM for intensity-modulated direct-detection systems," *J. Commun. and Info. Netws.*, vol. 2, no. 4, pp. 36–46, Dec. 2017. [Online]. Available: https://doi.org/10.1007/s41650-017-0035-5

[23] B. Ranjha and M. Kavehrad, "Hybrid asymmetrically clipped OFDM-based IM/DD optical wireless system," *IEEE/OSA J. Optical Commun. and Netw.*, vol. 6, no. 4, pp. 387–396, Apr. 2014.

[24] N. Wu and Y. Bar-Ness, "A novel power-efficient scheme asymmetrically and symmetrically clipping optical (ASCO)-OFDM for IM/DD optical systems," *EURASIP J. Advances in Signal Processing*, vol. 2015, no. 1, p. 3, Jan. 2015. [Online]. Available: https://doi.org/10.1186/1687-6180-2015-3

[25] M. S. Islim, D. Tsonev, and H. Haas, "On the superposition modulation for OFDM-based optical wireless communication," in *IEEE Global Conf. Signal and Info. Process.*, Dec. 2015, pp. 1022–1026.

[26] Q. Wang, C. Qian, X. Guo, Z. Wang, D. G. Cunningham, and I. H. White, "Layered ACO-OFDM for intensity-modulated direct-detection optical wireless transmission," *Opt. Express*, vol. 23, no. 9, pp. 12 382–12 393, May 2015.

[27] H. Elgala and T. D. C. Little, "See-ofdm: Spectral and energy efficient ofdm for optical im/dd systems," in *Annu. International Symp. on Pers., Indoor, and Mobile Radio Commun.*, Sep. 2014, pp. 851–855.

[28] M. M. A. Mohammed and Z. A. El-Sahn, "Enhanced asymmetrically clipped optical OFDM for next generation PONs," in *Asia Commun. and Photon. Conf. 2015.* Optical Society of America, 2015, p. ASu2A.73.

[29] D. Tsonev and H. Haas, "Avoiding spectral efficiency loss in unipolar OFDM for optical wireless communication," in *2014 IEEE Int. Conf. Commun., (ICC)*, June 2014, pp. 3336–3341.

[30] M. S. Islim, D. Tsonev, and H. Haas, "A generalized solution to the spectral efficiency loss in unipolar optical OFDM-based systems," in *2015 IEEE Int. Conf. Commun., (ICC)*, June 2015, pp. 5126–5131.

[31] A. S., *Visible Light Communication*, 1st ed., Sept. 2015.

[32] P. Haigh, H. L. Minh, and Z. Ghassemlooy, "Transmitter distribution for MIMO visible light communication systems," in *12th Annu. Post Graduate Symp. on the Convergence of Telecommun., Netw. and Broadcast.*, 2011. [Online]. Available: http://nrl.northumbria.ac.uk/7480/

[33] S. Long, M. A. Khalighi, M. Wolf, S. Bourennane, and Z. Ghassemlooy, "Investigating channel frequency selectivity in indoor visible-light communication systems," *IET Optoelectronics*, vol. 10, no. 3, pp. 80–88, May 2016.

[34] S. K. Wilson and J. Armstrong, "Transmitter and receiver methods for improving asymmetrically-clipped optical OFDM," *IEEE Trans. Wireless Commun.*, vol. 8, no. 9, pp. 4561–4567, Sep. 2009.

[35] Z. Ghassemlooy, F. Ebrahimi, S. Rajbhandari, S. Olyaee, X. Tang, and S. Zvanovec, "Investigation of a hybrid OFDM-PWM/PPM visible light communications system," in *Optics Commun.*, Aug. 2018.

[36] J. B. Carruthers and J. M. Kahn, "Modeling of nondirected wireless infrared channels," *IEEE Trans. Commun.*, vol. 45, no. 10, pp. 1260–1268, Oct. 1997.

[37] J. Kahn and J. Barry, "Wireless infrared communications," *Proc. IEEE*, vol. 85, no. 2, pp. 265–298, Feb. 1997.

[38] D. Tsonev, S. Sinanovic, and H. Haas, "Novel unipolar orthogonal frequency division multiplexing (U-OFDM) for optical wireless," in *Veh. Technol. Conf.*, May 2012, pp. 1–5.

[39] L. Chen, B. Krongold, and J. Evans, "Diversity combining for asymmetrically clipped optical OFDM in IM/DD channels," in *IEEE Global Commun. Conf. (GLOBECOM)*, Nov. 2009, pp. 1–6.

[40] H. Elgala, R. Mesleh, and H. Haas, "Practical considerations for indoor wireless optical system implementation using OFDM," in *Inter. Conf. Telecommun*, June 2009, pp. 25–29.

[41] X. Li, R. Mardling, and J. Armstrong, "Channel capacity of IM/DD optical communication systems and of ACO-OFDM," in *EEE Inter. Conf. Commun.*, June 2007, pp. 2128–2133.

[42] M. Ghavami, L. B. Michael, S. Haruyama, and R. Kohno, "A novel UWB pulse shape modulation system," *Wireless Personal Commun.*, vol. 23, no. 1, pp. 105–120, 2002.

[43] S. Arnon, "The effect of clock jitter in visible light communication applications," *J. Lightw. Technol.*, vol. 30, no. 21, pp. 3434–3439, 2012.